

# Thiophene-Bridged Double D- $\pi$ -A Dye for Efficient Dye-Sensitized Solar Cell

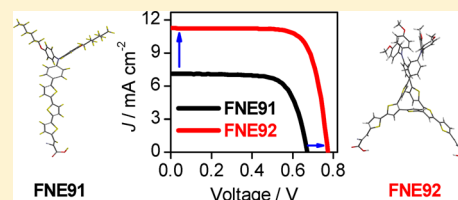
Xiaoming Ren, Shenghui Jiang, Mingyang Cha, Gang Zhou, and Zhong-Sheng Wang\*

Department of Chemistry &amp; Lab of Advanced Materials, Fudan University, 2205 Songhu Road, Shanghai 200438, P. R. China

## Supporting Information

**ABSTRACT:** An organic dye containing two D- $\pi$ -A branches linked with a thiophene unit has been designed and synthesized for efficient dye-sensitized solar cells (DSSCs). As compared to the rod-shape of the single D- $\pi$ -A analogue dye, the cross shape of the double D- $\pi$ -A branched dye is favorable for reducing intermolecular interaction and retarding charge recombination. Controlled intensity modulated photovoltage spectroscopy reveals that electron lifetime for the double D- $\pi$ -A dye-based DSSC is 14-fold longer than that for the corresponding single D- $\pi$ -A dye-based DSSC. Linking two D- $\pi$ -A branches with a thiophene unit increases open-circuit photovoltage by 100 mV and short-circuit photocurrent by 4.10 mA cm<sup>-2</sup>. As a consequence, power conversion efficiency is enhanced by about 2-fold. This work presents a new route to designing sensitizers with high suppression ability of charge recombination toward high-performance DSSCs.

**KEYWORDS:** double D- $\pi$ -A organic dye, dye-sensitized solar cells, charge recombination



## INTRODUCTION

As a promising alternative to silicon-based photovoltaic devices, dye-sensitized solar cells (DSSCs) have attracted much attention in both academic<sup>1</sup> and industrial fields<sup>2</sup> because of their low cost and easy production. To date, power conversion efficiencies greater than 11% have been achieved with ruthenium sensitizers.<sup>1a,3</sup> Recently, there has been a surge of research interest in organic sensitizers, because they have advantages such as high molar absorption coefficients, facile molecular tailoring, and cost-effectiveness.<sup>4</sup> Furthermore, the diversity in molecular structures offers infinite possibilities to tune the photophysical and electrochemical properties, which is favorable for the optimization of solar cell performance.

Most of efficient organic sensitizers have the donor- $\pi$ -bridge-acceptor (D- $\pi$ -A) structure, containing a donor such as diphenylamine (DPA),<sup>5</sup> carbazole,<sup>6</sup> indoline,<sup>7</sup> etc., a  $\pi$  conjugation bridge composed of thiophene,<sup>8</sup> methine,<sup>9</sup> benzene<sup>10</sup> units, etc., and an acceptor such as cyanoacrylic acid<sup>11</sup> or rhodanine-3-acetic acid.<sup>12</sup> The single D- $\pi$ -A sensitizer has a rod-like configuration, which may cause undesirable dye aggregation and charge recombination.<sup>13</sup> The close  $\pi$ - $\pi$  stacking of dye molecules can lead to self-quenching of excited states and hence inefficient electron injection.<sup>14</sup> One effective strategy for overcoming this problem is the introduction of long alkyl chains into the dye.<sup>15</sup> Employing starburst dyes with bulky multidonor can also suppress dye aggregation and block the charge recombination of injected electrons with acceptors in the electrolyte.<sup>16</sup>

To enhance optical density and binding strength of dye on the TiO<sub>2</sub>, of particular interest is the synthesis of dianchoring dye,<sup>17</sup> which is verified to enhance photocurrent due to the extended  $\pi$ -conjugated framework and higher molar extinction coefficient.<sup>17a,d</sup> Several dianchoring organic dyes have been

synthesized for use in DSSCs, and they have demonstrated better solar cell performance than the single D- $\pi$ -A analogue dyes due to the improved photoresponse and photocurrent.<sup>17a,d</sup> However, the open-circuit photovoltage for the reported dyes with two anchor groups is comparable to or lower than that for the analogue dyes with one anchor group.<sup>17b,c</sup> For example, Nazeeruddin et al. and Hagfeldt et al. designed and synthesized a double branched dye containing one donor (triphenylamine), two  $\pi$  bridges, and two anchors.<sup>17a,b</sup> Unfortunately, the dye with two anchor groups leads to more serious charge recombination, resulting in lower open-circuit photovoltage than the dye with one anchor group.<sup>17b</sup> Thus, the power conversion efficiency of the reported dyes with two anchors is limited by the low open-circuit photovoltage. If the double branched dye is endowed with an ability to suppress charge recombination, open-circuit photovoltage can be improved, and hence further improvement of power conversion efficiency can be anticipated. Therefore, new molecular design of double branched dyes is still important and interesting to optimize the dye structures for more efficient DSSCs.

In this study, we designed and synthesized a double D- $\pi$ -A dye FNE92 (Figure 1) with a thiophene unit bridging two same D- $\pi$ -A chains. The extended  $\pi$ -conjugation due to the conjugated linking of the two D- $\pi$ -A branches by a thiophene unit is expected to enhance molar extinction coefficient, and also the cross shape of the double D- $\pi$ -A dye and/or the crossing part (i.e., the thiophene linker) between the two branches would block triiodides approaching the TiO<sub>2</sub> surface for charge recombination. Experimental results indicate that the

Received: July 17, 2012

Revised: August 7, 2012

Published: August 7, 2012

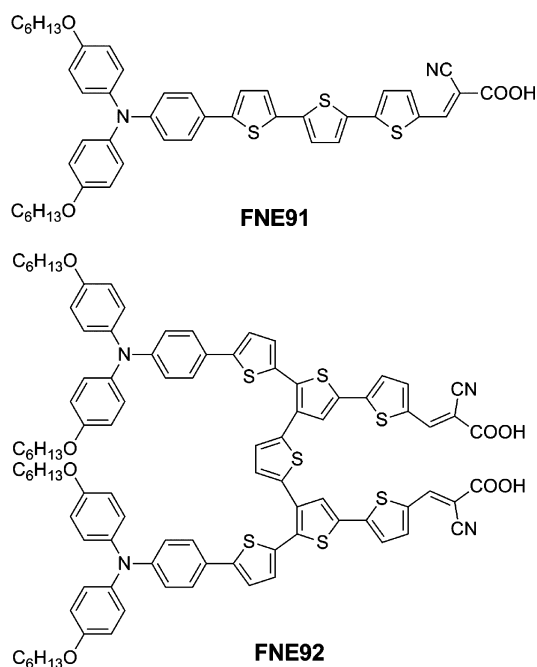


Figure 1. Structures of dyes FNE91 and FNE92.

double D- $\pi$ -A dye FNE92 produced much higher short-circuit photocurrent and open-circuit photovoltage than the single D- $\pi$ -A analogue dye FNE91. Controlled intensity modulated photovoltage spectroscopy and charge extraction have been carried out to clarify the factors affecting the open-circuit photovoltage.

## EXPERIMENTAL SECTION

**Materials and Reagents.** The syntheses of dyes FNE91 and FNE92 are detailed in the Supporting Information. Solvents were dried by standard procedures. Other chemicals and reagents were available from commercial sources and used without further purification. Transparent conductive glass (F-doped SnO<sub>2</sub>, FTO, 15  $\Omega$ /square, transmittance of 85%, Nippon Sheet Glass Co., Japan) was used as the substrate for the fabrication of TiO<sub>2</sub> thin film electrode.

**Fabrication of DSSCs.** TiO<sub>2</sub> films (10  $\mu$ m) consisting of a 6  $\mu$ m transparent layer ( $\sim$ 20 nm nanoparticles) and a 4  $\mu$ m scattering layer ( $\sim$ 100 nm particles) were prepared using a screen printing technique,<sup>18</sup> followed by sintering at 500  $^{\circ}$ C under an air flow. After cooling, the TiO<sub>2</sub> films were impregnated in a 0.05 M aqueous TiCl<sub>4</sub> solution for 30 min at 70  $^{\circ}$ C and then rinsed with deionized water. The TiCl<sub>4</sub>-treated TiO<sub>2</sub> films were annealed at 450  $^{\circ}$ C for 30 min and then cooled to 120  $^{\circ}$ C before immersed into the dye solution (0.3 mM in chloroform) for 16 h. After adsorption of the dyes, the electrodes were rinsed with chloroform and acetonitrile, respectively. The working and Pt-counter electrodes were assembled into a sealed sandwich solar cell with a thermoplastic frame (Surly 30  $\mu$ m thick). Redox electrolyte (0.6 M 1,2-dimethyl-3-n-propylimidazolium iodide, 0.1 M LiI, 0.05 M I<sub>2</sub>, and 0.5 M 4-tert-butylpyridine in dry acetonitrile) was introduced through the holes on the back of counter electrode. Finally, the two holes were sealed using additional hot melt Surlyn film covered with a thin glass slide under hot pressing.

**Characterizations.** <sup>1</sup>H NMR (400 MHz) and <sup>13</sup>C NMR (100 MHz) spectra were measured on a Varian Mercury Plus-400 spectrometer. The chemical shifts were expressed in ppm downfield from tetramethylsilane (TMS). IR spectra were recorded on a Shimadzu IRAffinity-1 spectrometer. UV-vis absorption spectra of dye solutions and dye-loaded films were recorded with a Shimadzu Model 2550 UV-vis spectrophotometer. Cyclic voltammetry (CV) measurements were performed with an Autolab analyzer using a typical three-electrode electrochemical cell in a solution of

tetrabutylammonium hexafluorophosphate (0.1M) in anhydrous acetonitrile with a scan rate of 50 mV s<sup>-1</sup> at room temperature under argon. Dye-loaded films, platinum, and Ag/Ag<sup>+</sup> electrode were employed as working, counter, and reference electrodes, respectively. The potential of the reference electrode was calibrated by ferrocene, and all potentials mentioned in this work are relative to normal hydrogen electrode (NHE). The film thickness was measured by a surface profiler (Veeco Dektak 150).

The current density-voltage ( $J$ - $V$ ) characteristics of DSSCs were recorded on a Keithley 2400 source meter under illumination of simulated AM1.5G solar light coming from a solar simulator (Oriol-94043A) equipped with a Xe lamp and an AM1.5G filter. The light intensity was calibrated using a standard Si solar cell (Newport 91150). A black mask with aperture area of 0.2304 cm<sup>2</sup> was used to avoid stray light. Action spectra of incident monochromatic photon-to-electron conversion efficiency (IPCE) as a function of wavelength were obtained with an Oriol-74125 system. The intensity of incident monochromatic light was measured with a Si detector (Oriol-71640).

The electron lifetimes were measured with controlled intensity modulated photovoltage spectroscopy (IMVS), and charge densities at open-circuit were measured using charge extraction technique. IMVS and charge extraction analysis were carried out on an electrochemical workstation (Zahner XPOT), which includes a green light-emitting diode (LED, 532 nm) and the corresponding control system. The intensity-modulated spectra were measured at room temperature with light intensity ranging from 0.5 to 45 W m<sup>-2</sup>, in modulation frequency ranging from 0.1 Hz to 10 kHz, and with modulation amplitude less than 5% of the light intensity.

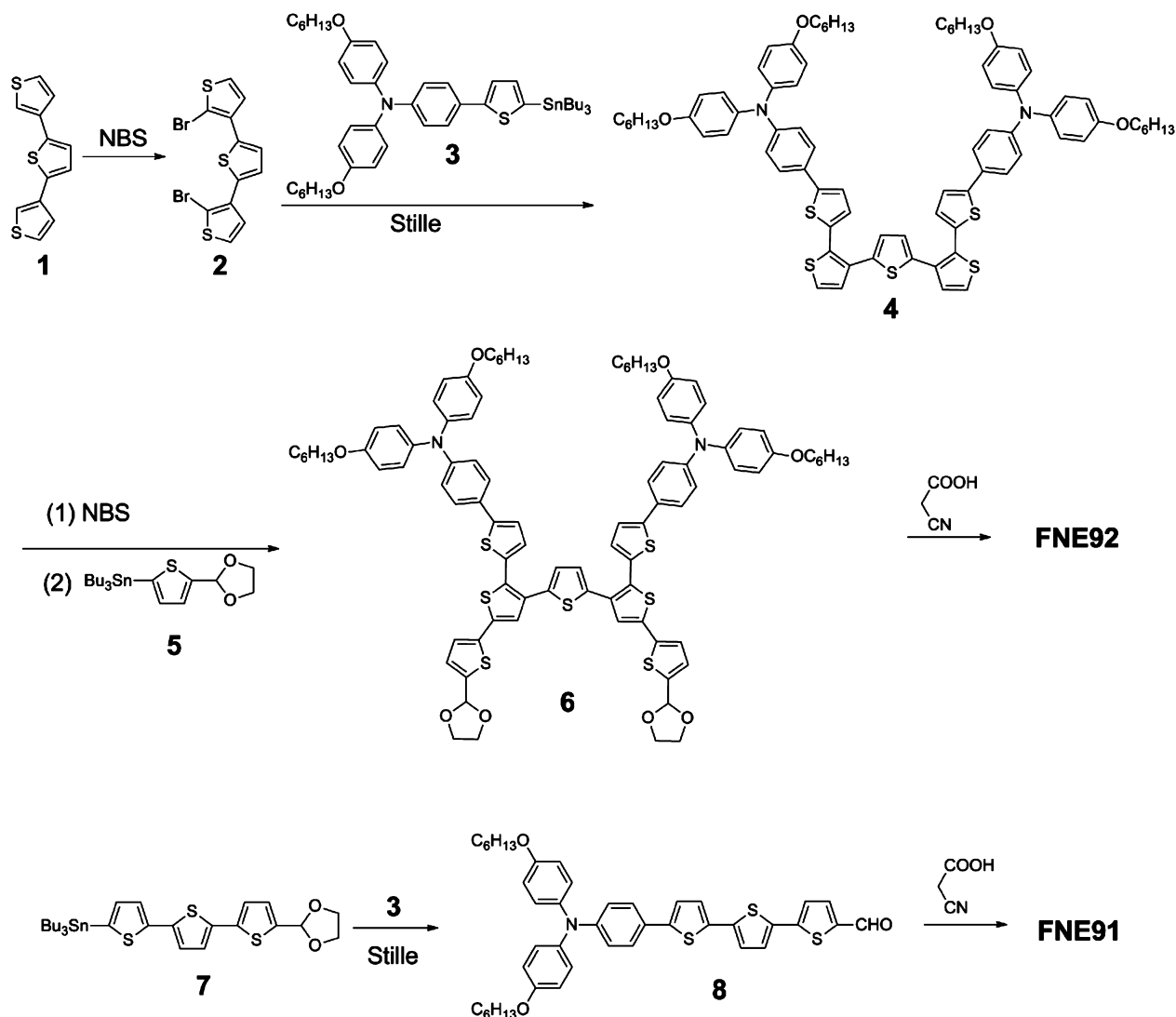
## RESULTS AND DISCUSSION

**Molecular Design and Synthesis.** The connection between two neighbored thiophene units in oligothiophenes includes  $\alpha$ - $\alpha$ ,  $\alpha$ - $\beta$ , or  $\beta$ - $\beta$  linkage. Generally,  $\alpha$ - $\alpha$  linkage provides a better  $\pi$ -electron conjugation, whereas  $\alpha$ - $\beta$  or  $\beta$ - $\beta$  linkage has nonplanar structure and therefore reduces the conjugation.<sup>19</sup> In this work, two terthiophene-based D- $\pi$ -A chains were connected via a thiophene core with two  $\alpha$ - $\beta$  linkage. Such  $\alpha$ - $\beta$  linkage not only retains the charge delocalization in each D- $\pi$ -A chain, but also provides a rigid configuration under the assistance of steric effect. As a result, our designed organic molecules can stand on the TiO<sub>2</sub> surface and therefore the intermolecular  $\pi$ - $\pi$  interactions can be reduced significantly, which greatly benefits to photocurrent generation.

For electron-releasing group (aryl or alkyl) substituted thiophene unit at 3-position, electrophilic substitution occurs regioselectively in 2-position of thiophene because of the inductive effect of 3-substitution.<sup>20</sup> Employing this regioselective strategy, donor and acceptor parts can be sequentially connected at 2- and 5-positions of the thiophene units. Herein, the double D- $\pi$ -A dye FNE92 was synthesized in five steps using  $\alpha$ - $\beta$  linked terthiophene **1** as the starting core (Scheme 1). After regioselective dibromination, compound **4** was obtained when two hexyloxy-substituted triphenylamine donor were attached into the twisted terthiophene backbone by Stille coupling.<sup>21</sup> Further dibromination by N-bromosuccinimide (NBS) and subsequent Stille coupling with (5'-(1,3-dioxolan-2-yl)-[2,2'-bithiophen]-5-yl)tributyl afforded 1, 3-dioxalane protected intermediate **5**. Finally, the tandem reaction of deprotection and Knoevenagel condensation<sup>22</sup> gave the target dye FNE92. For comparison, the reference dye FNE91 with a single D- $\pi$ -A chain was prepared similarly according to literatures.<sup>16c</sup>

**Dye Adsorption.** To investigate the anchoring properties of the dyes on the TiO<sub>2</sub> films, we carried out IR for the dye

Scheme 1. Synthetic Routes of Dyes FNE91 and FNE92



powders and dye-loaded  $\text{TiO}_2$  films, as shown in Figure S1 in the Supporting Information. Characteristic band at  $2216\text{ cm}^{-1}$  for cyano ( $\text{C}\equiv\text{N}$ ) was observed for both dye powders and dye-loaded  $\text{TiO}_2$  films.<sup>17a</sup> For dye powders, the carbonyl peaks were located at  $1684$  and  $1690\text{ cm}^{-1}$  for FNE91 and FNE92, respectively. Upon dye adsorption to the  $\text{TiO}_2$  surface, the carbonyl peaks disappeared, while instead asymmetric ( $\nu_{\text{as}}$ ,  $1603\text{ cm}^{-1}$  for FNE91 and  $1601\text{ cm}^{-1}$  for FNE92) and symmetric stretching ( $\nu_{\text{s}}$ ,  $1371\text{ cm}^{-1}$  for FNE91 and  $1367\text{ cm}^{-1}$  for FNE92) bands for carboxylate units appeared in the spectra.<sup>23</sup> This observation implies that FNE91 and FNE92 were chemically adsorbed onto the  $\text{TiO}_2$  surface via single- and double-anchoring modes, respectively. According to the Deacon Philips rule<sup>24</sup> and previous similar report,<sup>17a,b</sup> the dye molecules most likely adsorb on the  $\text{TiO}_2$  surface via a bidentate bridging binding mode.

**UV-Vis Absorption Properties.** Figure 2a shows the UV-vis absorption spectra of the two dye solutions in chloroform, and the corresponding data are summarized in Table 1. Two distinct bands were observed for both dyes. The band located at shorter wavelength is attributed to the  $\pi-\pi^*$  electron transition of the chromophore, and the other at longer wavelength is attributed to the intramolecular charge transfer

(ICT) from the donor to acceptor.<sup>25</sup> Owing to the extended  $\pi$  conjugation from single to double D- $\pi$ -A structure, molar extinction coefficient for the  $\pi-\pi^*$  electron transition band increases from  $2.8 \times 10^4\text{ M}^{-1}\text{ cm}^{-1}$  for the single branch to  $5.8 \times 10^4\text{ M}^{-1}\text{ cm}^{-1}$  for the double branch. On the contrary, the ICT band for FNE92 is slightly weaker than that for FNE91.<sup>17d</sup> The  $\pi-\pi^*$  electron transition band is less intense than the ICT band for the single branched dye FNE91, whereas the former is more intense than the latter for the double branched dye FNE92 so that the latter appears as a shoulder because of the peak overlapping. As shown in Figure 3, density functional calculations at B3LYP/6-31G\* level demonstrate that the two D- $\pi$ -A branches cross perpendicularly, which interrupts the coplanarity of the double D- $\pi$ -A branches, resulting in blue shifts for both absorption peaks as compared to the single D- $\pi$ -A branch (Table 1). The crossing of the two branches at the thiophene bridge in FNE92 probably weakens the charge communication so that the ICT band is weaker than the  $\pi-\pi^*$  electron transition band.

Figure 2b shows the UV-vis absorption spectra for the dye-loaded films. Upon dye adsorption on the  $\text{TiO}_2$  surface, the ICT band for FNE91 blue shifts to  $415\text{ nm}$ , because of the deprotonation of the anchoring group and/or the different

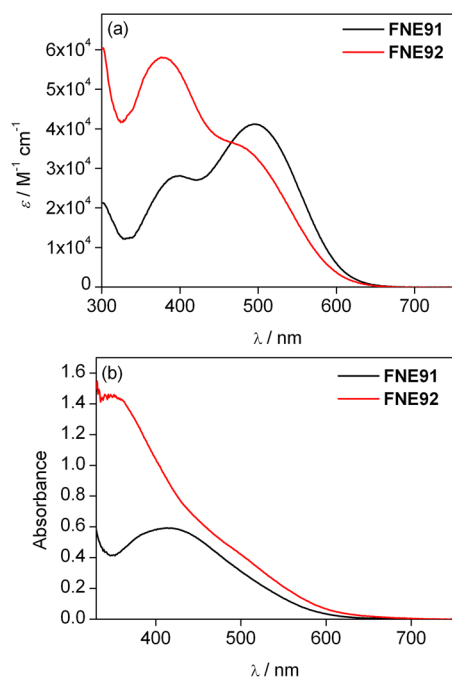


**Figure 2.** UV-vis absorption spectra of (a) dye solutions in chloroform and (b) dye-loaded  $\text{TiO}_2$  films (1  $\mu\text{m}$ ).

media polarity, whereas the  $\pi-\pi^*$  electron transition band disappears due to the peak overlapping. By contrast, the  $\pi-\pi^*$  electron transition band is observable while the ICT band disappeared because of the peak overlapping for the FNE92 dye-loaded  $\text{TiO}_2$  film. Although FNE92 has a larger molecular size than FNE91, the dye amount on the  $\text{TiO}_2$  (1  $\mu\text{m}$  thick) surface is similar for both dyes, as seen in Table 1. A more compact dye layer for FNE92 is formed on the  $\text{TiO}_2$  surface.

**Electrochemical Properties.** Energy levels of dye sensitizers are crucial to judge the possibilities of electron injection from the excited dye molecules to the conduction band of  $\text{TiO}_2$  and dye regeneration by the iodide. The oxidation potentials were measured by cyclic voltammetry (Figure 4). The highest occupied molecular orbital (HOMO) levels for both dyes, taken from the first oxidation potential, are calculated to be 0.88 V (vs NHE, the same below), which are more positive than the redox potential of the  $\text{I}^-/\text{I}_3^-$  redox couple ( $\sim 0.4$  V), ensuring sufficient driving force for reduction of oxidized dye molecules. Correspondingly, estimated from the band gap derived from the absorption onset for the dye-loaded  $\text{TiO}_2$  film and HOMO levels,<sup>26</sup> the lowest unoccupied molecular orbital (LUMO) energy levels for both dyes, approximately taken as the excited oxidation potentials, are calculated to be  $-1.07$  V. The LUMO levels are more negative than the conduction band edge of  $\text{TiO}_2$  ( $-0.66$  V in acetonitrile containing 0.1 M  $\text{LiClO}_4$ ),<sup>27</sup> suggesting a sufficient driving

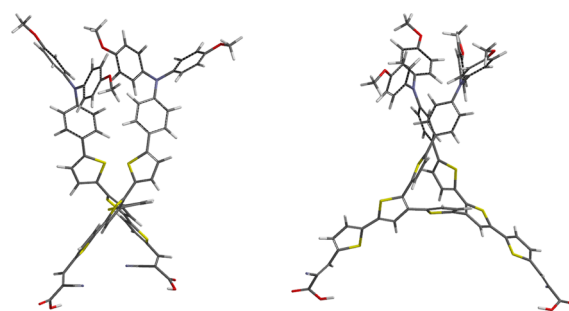


**Figure 3.** Front and side views of calculated chemical structure of dye FNE92.

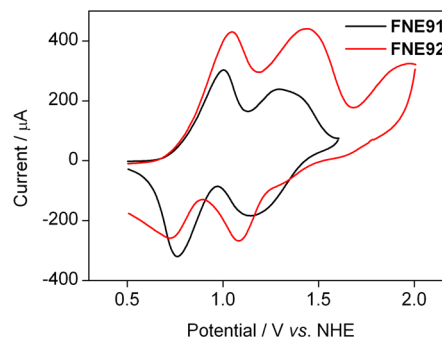


**Figure 4.** Cyclic voltammograms of FNE91- and FNE92-loaded  $\text{TiO}_2$  films.

force for electron injection from the excited dye molecules to the conduction band of  $\text{TiO}_2$ .

**Solar Cell Performance.** Incident photon-to-electron conversion efficiencies (IPCE) as a function of incident wavelength for the DSSCs based on the resulting organic dyes on  $\text{TiO}_2$  films are plotted in Figure 5. FNE91 shows an

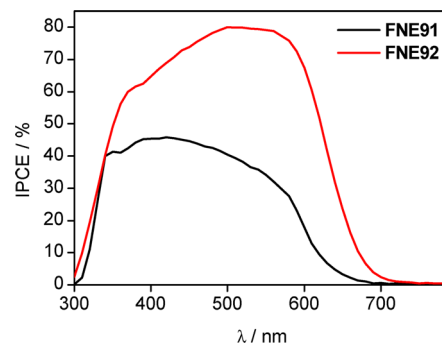


**Figure 5.** IPCE spectra for DSSCs based on FNE91 or FNE92 in the absence of deoxycholic acid.

**Table 1.** Photophysical and Electrochemical Properties of Dyes FNE91 and FNE92

dye	absorption		dye loading <sup>b</sup> ( $10^{-8}$ mol $\text{cm}^{-2}$ )	HOMO <sup>c</sup> (V vs NHE)	gap <sup>d</sup> (eV)	LUMO <sup>e</sup> (V vs NHE)
	$\lambda_{\text{max}}$ <sup>a</sup> (nm)	$\epsilon$ at $\lambda_{\text{max}}$ ( $10^4 \text{ M}^{-1} \text{cm}^{-1}$ )				
FNE91	395, 495	2.8, 4.1	2.6	0.88	1.95	$-1.07$
FNE92	380, 480	5.8, 3.6	2.8	0.88	1.95	$-1.07$

<sup>a</sup>Absorption maximum in chloroform solution. <sup>b</sup>The dye loading was determined from a dye-loaded 1  $\mu\text{m}$  thick  $\text{TiO}_2$  film. <sup>c</sup>The HOMO was taken from the first redox potential in CV plot. <sup>d</sup>The gap is estimated from the absorption onset of the dye-loaded  $\text{TiO}_2$  film. <sup>e</sup>The LUMO was calculated with the expression of  $\text{LUMO} = \text{HOMO} - \text{Gap}$ .

IPCE maximum of 46%, while FNE92 shows an IPCE maximum of 80%. As the two dyes have same HOMO and LUMO energy levels and the latter is sufficiently high for electron injection, the different IPCE values may result from the different shape of the two dyes considering that light-harvesting efficiency is close to 100% for the dye-loaded 10- $\mu\text{m}$  films. FNE91 has a rod shape and reasonably has strong intermolecular  $\pi$ - $\pi$  interaction, which leads to self-quenching of excited states and hence inefficient electron injection. As a result, FNE91-based DSSC produces lower IPCE than expected. By contrast, FNE92 has a cross shape and reasonably has weak intermolecular  $\pi$ - $\pi$  interaction. Therefore, FNE92-based DSSC generates unity maximum IPCE. To verify the difference of intermolecular  $\pi$ - $\pi$  interaction, effect of coadsorption with deoxycholic acid (20 mM in dye solution) was investigated for both dyes. The experimental result indicates that coadsorption is effective to improve IPCE significantly for FNE91 (see Figure S2 in the Supporting Information) but ineffective for FNE92. This indicates that the two long hexyloxy groups attached on the donor part in the single D- $\pi$ -A structure cannot exhibit the efficient antiaggregation effect,<sup>28</sup> whereas the double D- $\pi$ -A dye FNE92 with a cross structure is effective at reducing the intermolecular  $\pi$ - $\pi$  interaction and therefore improving IPCE.

The current-voltage characteristics of DSSCs were tested under simulated AM1.5G illumination (100  $\text{mW cm}^{-2}$ ). Figure 6 illustrates the  $J$ - $V$  curves and the performance parameters are

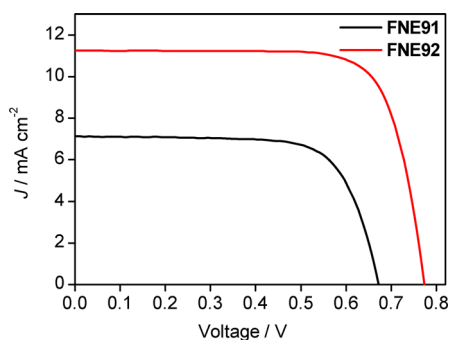


**Figure 6.**  $J$ - $V$  curves for DSSCs based on FNE91 or FNE92 in the absence of deoxycholic acid.

listed in Table 1. The FNE91-based DSSC produced a  $J_{sc}$  of 7.13  $\text{mA cm}^{-2}$ , a  $V_{oc}$  of 0.67 V, and an  $FF$  of 0.71, corresponding to an  $\eta$  of 3.4%. Under the same condition, the DSSC based on FNE92 offered a  $J_{sc}$  of 11.25  $\text{mA cm}^{-2}$ , a  $V_{oc}$  of 0.77 V, and an  $FF$  of 0.76, corresponding to an  $\eta$  of 6.6%. The  $J_{sc}$  is improved by 4.10  $\text{mA cm}^{-2}$ ,  $V_{oc}$  is lifted by 0.10 V, and the  $\eta$  is enhanced by 94% from FNE91 to FNE92. The difference in  $J_{sc}$  is consistent with the IPCE trend as shown in Figure 5. The increase in  $V_{oc}$  by 0.10 V from the single to double D- $\pi$ -A branched dye can be explained by the analyses of conduction band (CB) position and charge recombination rate.

Figure 7 shows the relation between  $V_{oc}$  and extracted charge density ( $Q$ ) at open circuit. At a fixed  $Q$ , an increased  $V_{oc}$  indicates a negative shift of CB, and a decreased  $V_{oc}$  means a positive shift of CB.<sup>29</sup> As compared to FNE91-based DSSC, FNE92-based DSSC showed a downward CB shift by 30 mV. The positive shift of CB is likely caused by more protons present on  $\text{TiO}_2$  surface for FNE92,<sup>27</sup> because both dyes have similar adsorbed amount on the  $\text{TiO}_2$  surface but one FNE92 molecule contains two carboxylic acids while one FNE91

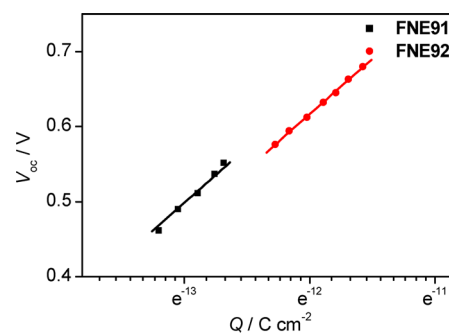


**Figure 7.**  $V_{oc}$  as a function of charge density at open circuit for DSSCs with FNE91 or FNE92. Three identical devices were tested in each case with standard deviation less than 5%.

molecule contains only one. Upon dye adsorption, the protons were first dissociated from carboxylic acid groups, but the dissociated protons mostly stay on the  $\text{TiO}_2$  surface due to the interaction of proton and hydroxyl groups on  $\text{TiO}_2$  though we cannot determine how much percentage of the protons is present on the surface.

As a positive shift of CB should lead to a decrease in  $V_{oc}$ , the observed higher  $V_{oc}$  for FNE92 should be attributed to retarded charge recombination, to be discussed next. Figure 8 shows the

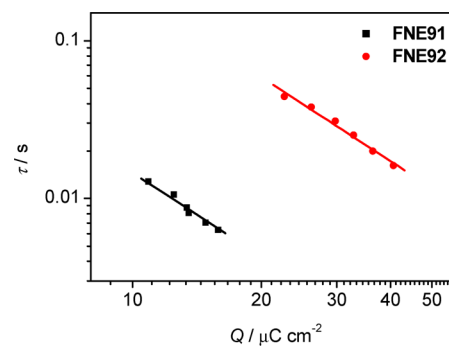


**Figure 8.** Electron lifetime against charge density for FNE91- and FNE92-based DSSCs. Three identical devices were tested in each case with standard deviation less than 5%.

electron lifetime against charge density for FNE91- and FNE92-based DSSCs. At the same charge density, the electron lifetime of FNE92-based DSSC is longer than that of FNE91-based DSSC by 14-fold. This indicates that charge recombination between electrons in  $\text{TiO}_2$  film and electron acceptors in the electrolyte is significantly retarded by the double D- $\pi$ -A branched dye as compared to the single D- $\pi$ -A branched dye. At 45  $\text{W m}^{-2}$  LED light (532 nm), the extracted charge densities are 16.1 and 34.6  $\mu\text{C cm}^{-2}$  for FNE91 and FNE92-based DSSCs, respectively. The higher charge density for FNE92 is attributed to the longer electron lifetime and higher  $J_{sc}$  as well. According to the  $Q$ - $V_{oc}$  plot, the  $V_{oc}$  gain arising solely from the increased charge density or retarded charge recombination is 113 mV. Thus, the collective effect of CB shift and retarded charge recombination rate is 83 mV (= 113 mV - 30 mV) increase in  $V_{oc}$ , in good agreement with the experimentally observed  $V_{oc}$  increase (90 mV) under 45  $\text{W m}^{-2}$  LED light (532 nm). Therefore, it is concluded that the observed enhancement of  $V_{oc}$  from single- to double-branched dye is attributed to the collective effect of retarded charge recombination and positive shift of CB.

Based on the optimized geometrical structure of the two dyes, FNE91 has a rod shape, whereas FNE92 has a cross shape (Figure 3). When the dye molecules were adsorbed on the TiO<sub>2</sub> surface, the cross structure for FNE92 can block triiodides approaching the TiO<sub>2</sub> surface for charge recombination, while the rod shape for FNE91 may remain some larger gaps between molecules so that triiodides can approach the TiO<sub>2</sub> surface easier for charge recombination. As a consequence, much longer electron lifetime and higher  $V_{oc}$  are observed for FNE92 with a cross structure than those for FNE91. By comparison with some reported dyes (NKX-2677,<sup>26</sup> MK-2,<sup>6</sup> and the standard N719 dye,<sup>3b</sup> see Figure S3 in the Supporting Information), the double D- $\pi$ -A dye FNE92 also exhibits advantage in the generation of high  $V_{oc}$ . We have prepared DSSCs with the above-mentioned reported dyes for direct comparison with the DSSCs based on FNE91 and FNE92 under the same conditions, and the results are summarized in Table 2. NKX-2677 having no alkyl chains

**Table 2. Photovoltaic Performance Parameters for DSSCs with Various Dye Sensitizers**

	$J_{sc}$ (mA cm <sup>-2</sup> )	$V_{oc}$ (V)	FF	$\eta$ (%)	$\epsilon(10^4 \text{ M}^{-1} \text{ cm}^{-1})$ ( $\lambda_{max}/$ nm)
NKX-2677	9.63	0.60	0.75	4.3	6.4 (511)
MK-2	11.96	0.71	0.72	6.1	3.8 (480)
FNE91	7.13	0.67	0.71	3.4	4.1 (495)
FNE92	11.25	0.77	0.76	6.6	3.6 (480)
N719	11.22	0.74	0.75	6.2	1.3 (535)

suffers from serious dye aggregation and thus produces low  $V_{oc}$  and  $\eta$ . When alkyl chains are linked to the thiophene bridge for MK-2 or to the donor part for FNE91, higher  $V_{oc}$  is produced. The  $V_{oc}$  obtained from FNE92 is the highest for the dyes tested, and it is even higher than that obtained from N719 under the same conditions.

Long-term stability is one of the critical parameters for practical applications. Sealed DSSCs with a quasi-solid-state gel electrolyte (0.1 M LiI, 0.1 M I<sub>2</sub>, 0.1 M 4-*tert*-butylpyridine and 0.6 M 1,2-dimethyl-3-propylimidazolium iodide in 3-methoxypropionitrile gelled with 5 wt % poly(vinylidene fluoride-co-hexafluoropropylene) at open-circuit equipped with a 400 nm cutoff filter were subjected to continuous light soaking (100 mW cm<sup>-2</sup>, device surface temperature was ~50 °C). Figure 9 displays the evolution of photovoltaic performance parameters of FNE92-based quasi-solid-state DSSC under one sun soaking over a period of 1000 h.  $V_{oc}$  and FF experienced small fluctuations, whereas  $J_{sc}$  remained almost constant up to 370 h followed by a slight decrease (<4%) with time. As a result, the performance of the quasi-solid-state DSSC reached the best ( $V_{oc} = 0.67$  V,  $J_{sc} = 13.58$  mA cm<sup>-2</sup>, FF = 0.63,  $\eta = 5.7\%$ ) at 170 h and then decreased a little (<5%). FNE92-based quasi-solid-state DSSCs demonstrated good long-term stability during visible light soaking.

## CONCLUSIONS

In summary, we have designed and synthesized a thiophene bridged double D- $\pi$ -A dye FNE92, which has much stronger  $\pi$ - $\pi^*$  electron transition band than its monobranched analogue dye FNE91. The cross structure of FNE92 reduces intermolecular  $\pi$ - $\pi$  interaction and is thus favorable for electron injection and hence photocurrent generation. The

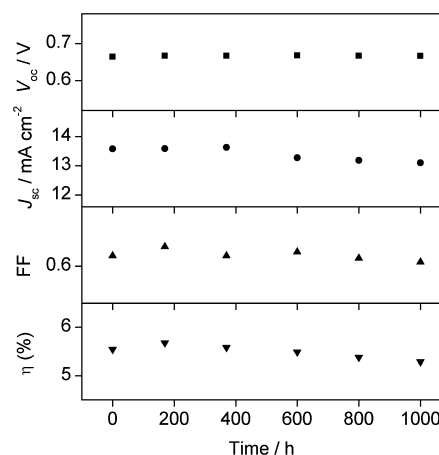


**Figure 9.** Evolutions of photovoltaic performance parameters for FNE92-based quasi-solid-state DSSC under one sun soaking.

cross structure also blocks triiodides approaching the TiO<sub>2</sub> surface, and therefore electron lifetime is enhanced remarkably at the same charge density compared to the rod-shaped monobranched analogue dye. In addition, the double-branched dye causes a downward displacement of CB compared to the single-branched dye. The collective effect of the CB shift and retarded charge recombination rate can account for the observed  $V_{oc}$  enhancement from mono- to dibranched dye. This finding presents a new route to designing sensitizers toward weak intermolecular  $\pi$ - $\pi$  interaction and slow charge recombination.

## ASSOCIATED CONTENT

### Supporting Information

Syntheses and characterizations of the sensitizers FNE91 and FNE92 by <sup>1</sup>H NMR, <sup>13</sup>C NMR, and HRMS. This material is available free of charge via the Internet at <http://pubs.acs.org>.

## AUTHOR INFORMATION

### Corresponding Author

\*E-mail: [zs.wang@fudan.edu.cn](mailto:zs.wang@fudan.edu.cn).

### Notes

The authors declare no competing financial interest.

## ACKNOWLEDGMENTS

This work was financially supported by the National Basic Research Program (No. 2011CB933302) of China, National Natural Science Foundation of China (20971025, 90922004, and 50903020), Shanghai Pujiang Program (11PJ1401700), Jiangsu Major Program (BY2010147), Shanghai Leading Academic Discipline Project(B108), and the Project sponsored by SRF for ROCS, SEM.

## REFERENCES

- (1) (a) Yella, A.; Lee, H. W.; Tsao, H. N.; Yi, C.; Chandiran, A. K.; Nazeeruddin, M. K.; Diau, E. W. -G.; Yeh, C. -Y.; Zakeeruddin, M. K.; Grätzel, M. *Science* **2011**, *334*, 629–634. (b) Hagfeldt, A.; Boschloo, G.; Sun, L.; Kloo, L.; Pettersson, H. *Chem. Rev.* **2010**, *110*, 6595–6663. (c) Cai, N.; Moon, S. J.; Cevey-Ha, L.; Moehl, T.; Humphry-Baker, R.; Wang, P.; Zakeeruddin, S. M.; Grätzel, M. *Nano Lett.* **2011**, *11*, 1452–1456. (d) Bai, Y.; Zhang, J.; Zhou, D.; Wang, Y.; Zhang, M.; Wang, P. *J. Am. Chem. Soc.* **2011**, *133*, 11442–11445. (e) Chen, T.; Wang, S.; Yang, Z.; Feng, Q.; Sun, X.; Li, L.; Wang, Z.-S.; Peng, H. *Angew. Chem., Int. Ed.* **2011**, *50*, 1815–1819. (f) Huang, Q.; Zhou, G.;

- Fang, L.; Hu, L.; Wang, Z.-S. *Energy Environ. Sci.* **2011**, *4*, 2145–2151.
- (g) Wang, H.; Zhang, X.; Gong, F.; Zhou, G.; Wang, Z.-S. *Adv. Mater.* **2012**, *24*, 121–124. (h) O'Regan, B.; Grätzel, M. *Nature* **1991**, *353*, 737–740. (i) Choi, H.; Lee, J. K.; Song, K. H.; Song, K.; Kang, S. O.; Ko, J. *Tetrahedron* **2007**, *63*, 1553–1559.
- (2) (a) Han, L.; Fukui, A.; Chiba, Y.; Islam, A.; Komiyama, R.; Fuke, N.; Koide, N.; Yamanaka, R.; Shimizu, M. *Appl. Phys. Lett.* **2009**, *94*, 013305/1–013305/3. (b) Gaudiana, R. *J. Phys. Chem. Lett.* **2010**, *1*, 1288–1289. (c) Späth, M.; Sommeling, P. M.; vanRoosmalen, J. A. M.; Smit, H. J. P.; vanderBurg, N. P. G.; Mahieu, D. R.; Bakker, N. J.; Kroon, J. M. *Prog. Photovolt.* **2003**, *11*, 207–220. (d) Wu, J.; Xiao, Y.; Tang, Q.; Yue, G.; Lin, J.; Huang, M.; Huang, Y.; Fan, L.; Lan, Z.; Yin, S.; Sato, T. *Adv. Mater.* **2012**, *24*, 1884–1888.
- (3) (a) Nazeeruddin, M. K.; Kay, A.; Rodicio, I.; Humphry-Baker, R.; Mueller, E.; Liska, P.; Vlachopoulos, N.; Grätzel, M. *J. Am. Chem. Soc.* **1993**, *115*, 6382–6390. (b) Nazeeruddin, M. K.; De Angelis, F.; Fantacci, S.; Selloni, A.; Viscardi, G.; Liska, P.; Ito, S.; Takeru, B.; Grätzel, M. G. *J. Am. Chem. Soc.* **2005**, *127*, 16835–16847. (c) Chen, C.; Wang, M.; Li, J.; Pootrakulchote, N.; Alibabaei, L.; Ngoc-le, C.; Decoppet, J.; Tsai, J.; Grätzel, C.; Wu, C.; Zakeeruddin, S. M.; Grätzel, M. *ACS Nano* **2009**, *3*, 3103–3109.
- (4) Mishra, A.; Fischer, M. K. R.; Bauerle, P. *Angew. Chem., Int. Ed.* **2009**, *48*, 2474–2499.
- (5) (a) Yum, J. H.; Hagberg, D. P.; Moon, S. J.; Karlsson, K. M.; Marinado, T.; Sun, L. C.; Hagfeldt, A.; Nazeeruddin, M. K.; Grätzel, M. *Angew. Chem., Int. Ed.* **2009**, *48*, 1576–1580. (b) Zhang, G.; Bala, H.; Cheng, Y.; Shi, D.; Lv, X.; Yu, Q.; Wang, P. *Chem. Commun.* **2009**, 2198–2200. (c) Choi, H.; Baik, C.; Kang, S. O.; Ko, J.; Kang, M. S.; Nazeeruddin, M. K.; Grätzel, M. *Angew. Chem., Int. Ed.* **2008**, *47*, 327–330. (d) Qu, S.; Hua, J.; Tian, H. *Science China Chem.* **2012**, *55*, 677–697. (e) Ning, Z.; Fu, Y.; Tian, H. *Energy Environ. Sci.* **2010**, *3*, 1170–1181. (f) Ning, Z.; Zhang, Q.; Pei, H.; Luan, J.; Lu, C.; Cui, Y.; Tian, H. *J. Phys. Chem. C* **2009**, *113*, 10307–10313.
- (6) Koumura, N.; Wang, Z.-S.; Mori, S.; Miyashita, M.; Suzuki, E.; Hara, K. *J. Am. Chem. Soc.* **2006**, *128*, 14256–14257.
- (7) (a) Kuang, D.; Uchida, S.; Humphry-Baker, R.; Zakeeruddin, S. M.; Grätzel, M. *Angew. Chem., Int. Ed.* **2008**, *47*, 1923–1927. (b) Howie, W. H.; Claeysens, F.; Miura, H.; Peter, L. M. *J. Am. Chem. Soc.* **2008**, *130*, 1367–1375. (c) Zhu, W.; Wu, Y.; Wang, S.; Li, W.; Li, X.; Chen, J.; Wang, Z.-S.; Tian, H. *Adv. Funct. Mater.* **2011**, *21*, 756–763. (d) Wu, Y.; Marszalek, M.; Zakeeruddin, S. M.; Zhang, Q.; Tian, H.; Grätzel, M.; Zhu, W. *Energy Environ. Sci.* **2012**, *5*, 8261–8272.
- (8) Choi, H.; Baik, C.; Kang, S. O.; Ko, J.; Kang, M. S.; Nazeeruddin, M. K.; Grätzel, M. *Angew. Chem., Int. Ed.* **2008**, *47*, 327–330.
- (9) Hara, K.; Sato, T.; Katoh, R.; Furube, A.; Yoshihara, T.; Murai, M.; Kurashige, M.; Ito, S.; Shinpo, A.; Suga, S.; Arakawa, H. *Adv. Funct. Mater.* **2005**, *15*, 246–252.
- (10) (a) Hagberg, D. P.; Edvinsson, T.; Marinado, T.; Boschloo, G.; Hagfeldt, A.; Sun, L. C. *Chem. Commun.* **2006**, 2245–2247. (b) Haid, S.; Marszalek, M.; Mishra, A.; Wielopolski, M.; Teuscher, J.; Moser, J.-E.; Humphry-Baker, R.; Zakeeruddin, S. M.; Grätzel, M.; Bäuerle, P. *Adv. Funct. Mater.* **2012**, *22*, 1291–1302.
- (11) Hara, K.; Kurashige, M.; Ito, S.; Shinpo, A.; Suga, S.; Sayama, K.; Arakawa, H. *Chem. Commun.* **2003**, 252–253.
- (12) Horiuchi, T.; Miura, H.; Uchida, S. *Chem. Commun.* **2003**, 3036–3037.
- (13) Hagberg, D. P.; Marinado, T.; Karlsson, K. M.; Nonomura, K.; Qin, P.; Boschloo, G.; Brinck, T.; Hagfeldt, A.; Sun, L. *J. Org. Chem.* **2007**, *72*, 9550–9556.
- (14) Liu, D.; Fessenden, R. W.; Hug, G. L.; Kamat, P. V. *J. Phys. Chem. B* **1997**, *101*, 2583–2590.
- (15) Wang, Z.-S.; Koumura, N.; Cui, Y.; Takahashi, M.; Sekiguchi, H.; Mori, A.; Kubo, T.; Furube, A.; Hara, K. *Chem. Mater.* **2008**, *20*, 3993–4003.
- (16) (a) Hagberg, D. P.; Yum, J. H.; Lee, H.; DeAngelis, F.; Marinado, T.; Karlsson, K. M.; Humphry-Baker, R.; Sun, L. C.; Hagfeldt, A.; Grätzel, M.; Nazeeruddin, M. K. *J. Am. Chem. Soc.* **2008**, *130*, 6259–6266. (b) Ning, Z. J.; Zhang, Q.; Wu, W. J.; Pei, H. C.; Liu, B.; Tian, H. *J. Org. Chem.* **2008**, *73*, 3791–3797. (c) Thomas, K. R. J.; Hsu, Y. C.; Lin, J. T.; Lee, K. M.; Ho, K. C.; Lai, C. H.; Cheng, Y. M.; Chou, P. T. *Chem. Mater.* **2008**, *20*, 1830–1840.
- (17) (a) Abboto, A.; Manfredi, N.; Marini, C.; Angelis, F. D.; Mosconi, E.; Yum, J.-H.; Zhang, X.; Zakeeruddin, S. M.; Grätzel, M. *Energy Environ. Sci.* **2009**, *2*, 1094–1101. (b) Jiang, X.; Karlsson, K. M.; Gabrielsson, E.; Johansson, E. M. J.; Quintana, M.; Karlsson, M.; Sun, L.; Boschloo, G.; Hagfeldt, A. *Adv. Funct. Mater.* **2011**, *21*, 2944–2952. (c) Liu, J.; Zhang, J.; Xu, M.; Zhou, D.; Jing, X.; Wang, P. *Energy Environ. Sci.* **2011**, *4*, 3021–3029. (d) Cao, D.; Peng, J.; Hong, Y.; Fang, X.; Wang, L.; Meier, H. *Org. Lett.* **2011**, *13*, 1610–1613. (e) Heredia, D.; Natera, J.; Gervald, M.; Otero, L.; Fungo, F.; Lin, C.-Y.; Wong, K.-T. *Org. Lett.* **2010**, *12*, 12–15. (f) Hong, Y.; Liao, J.-Y.; Cao, D.; Zang, X.; Kuang, D.-B.; Wang, L.; Meier, H.; Su, C.-Y. *J. Org. Chem.* **2011**, *76*, 8015–8021.
- (18) Wang, Z.-S.; Kawauchi, H.; Kashima, T.; Arakawa, H. *Coord. Chem. Rev.* **2004**, *248*, 1381–1389.
- (19) Xia, C.; Fan, X.; Locklin, J.; Advincula, R. C.; Gies, A.; Nonidez, W. *J. Am. Chem. Soc.* **2004**, *126*, 8735–8743.
- (20) (a) Clementi, S.; Marino, G. *Tetrahedron* **1969**, *25*, 4599–4603. (b) Clark, D. T. *Tetrahedron* **1968**, *24*, 2567–2573.
- (21) Milstein, D.; Stille, J. K. *J. Am. Chem. Soc.* **1978**, *100*, 3636–3638.
- (22) Knoevenagel, E. *Ber. Deutsch. Chem. Gesell.* **1898**, *31*, 2596–2619.
- (23) Tian, H.; Yang, X.; Chen, R.; Zhang, R.; Hagfeldt, A.; Sun, L. *J. Phys. Chem. C* **2008**, *112*, 11023–11033.
- (24) Deacon, G. B.; Phillips, R. J. *Coord. Chem. Rev.* **1980**, *33*, 227–250.
- (25) Roquet, S.; Cravino, A.; Leriche, P.; Alévêque, O.; Frère, P.; Roncali, J. *J. Am. Chem. Soc.* **2006**, *128*, 3459–3466.
- (26) Hara, K.; Wang, Z.-S.; Sato, T.; Furube, A.; Katoh, R.; Sugihara, H.; Dan-oh, Y.; Kasada, C.; Shinpo, A.; Suga, S. *J. Phys. Chem. B* **2005**, *109*, 15476–15482.
- (27) Redmond, G.; Fitzmaurice, D. *J. Phys. Chem.* **1993**, *97*, 1426–1430.
- (28) Liu, B.; Liu, Q. L.; You, D. Y.; Li, X.; Naruta, Y.; Zhu, W. *J. Mater. Chem.* **2012**, *22*, 13348–13356.
- (29) Kopidakis, N.; Neale, N. R.; Frank, A. J. *J. Phys. Chem. B* **2006**, *110*, 12485–12489.